



Short communication

A new cobalt triangular prism supramolecular flask: Encapsulation of a quinhydrone cofactor for hydrogenation of nitroarenes with high selectivity and efficiency

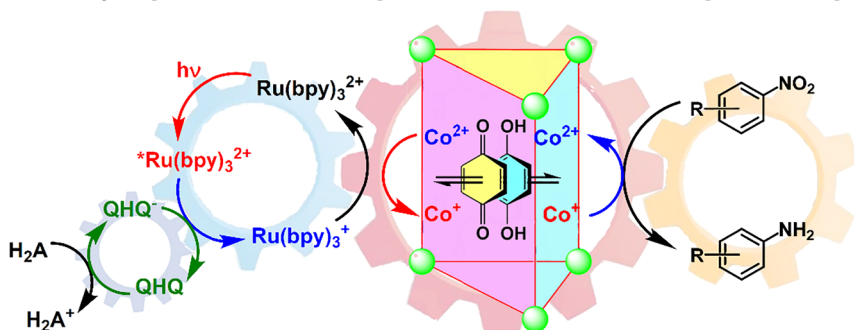
Sijia Zheng, Liang Zhao*, Jianwei Wei, Cheng He, Guangzhou Liu, Chunying Duan

State Key Laboratory of Fine Chemicals, Dalian University of Technology, Dalian 116024, PR China



GRAPHICAL ABSTRACT

A metal-organic prism with suitable redox potential was constructed for the encapsulation of a quinhydrone cofactor to selectively reduce nitroarenes.



ABSTRACT

A new M_6L_3 metal-organic triangular prism host $Co-L^1$ was synthesized that contains a sufficiently large cavity for encapsulation of a quinhydrone (QH₂) electron transporter to form charge-transfer complexes for accelerating electron delivery. Through the strong coordinating ability of the ONP chelator, a suitable redox potential was obtained for the combination of light-driven proton reduction with the selective hydrogenation of nitro groups. The experimental results showed that the regulation of redox potential is very beneficial for hydrogen production and that the introduction of QH₂ accelerates electron transfer and increases the reaction rate. Control experiments based on an inhibitor and a mononuclear compound resembling the cobalt corner of the triangular prism suggest enzyme-like behaviour. This synthetic platform, in which the supramolecular systems exhibit high activity and stability, provides an alternative strategy to selectively hydrogenate nitroarenes using light as a clean energy source.

1. Introduction

Functional aromatic amines are one of the most important intermediates and are widely used in dyes, agrochemicals and pharmaceutical synthesis [1,2]. They can be prepared by reductive amination [3], reduction of nitriles [4,5] and direct amination of alcohols [6,7]. The challenge for these methods is the selectivity of nitroarene reduction due to the influence of the multiple unsaturated functional groups of

accessible nitroarenes, which presents a serious obstacle to realizing the specific selective hydrogenation of nitro groups. Although various catalysts have been designed and synthesized for achieving highly efficient and selective hydrogenation of nitro groups [8,9], some of them still face considerable difficulties and challenges in practical production, including limited substrate scope, depletion of conventional energy and the danger of handling high-pressure hydrogen gas as a hydrogen source.

* Corresponding author.

E-mail address: zhaol@dlut.edu.cn (L. Zhao).<https://doi.org/10.1016/j.inoche.2019.107558>

Received 2 August 2019; Received in revised form 23 August 2019; Accepted 29 August 2019

Available online 30 August 2019

1387-7003/ © 2019 Elsevier B.V. All rights reserved.

In recent years, simulating enzymes in nature and using clean energy to realize chemical transformations under mild environmental conditions have been widely researched [10–13]. To attain the high efficiency and selectivity of enzymatic systems, chemists have used metal-organic hosts with defined hydrophobic cavities to mimic the remarkable properties of enzyme pockets for catalysing unique chemical transformations [14–19]. On the other hand, nature has developed untold millions of redox systems, in which redox processes are catalysed by numerous species of enzymes in the presence of the corresponding cofactors [20–23]. Among these cofactors, as a coenzyme, quinoxaline (QH) can effectively transfer electrons and protons through redox cycling between its oxidation state and reduced state [24].

Recently, we constructed an artificial charge-transfer complex system by encapsulating a QHQ cofactor for the photocatalytic generation of hydrogen in combination with the hydrogenation of nitrobenzene [25]. This previous study discussed that the formation of host-guest systems and changes in the overpotential of the metal sites influenced the efficiency of the light-driven hydrogen production and the hydrogenation of nitrobenzene. The results indicated that the cobalt-based metal-organic triangular prism with CH_2 centres has prominent advantages for the formation of host-guest systems and catalytic performance. In this work, the intrinsic redox potential of the cobalt-based metal-organic triangular prism, the electron transfer of QHQ outside the cavity and the reduction selectivity of nitro compounds were considered. By introducing four strong ONP chelators on the CH_2 -centred ligand to replace the previously reported ONN chelators, we assembled herein a new redox-active cobalt-based metal-organic triangular prism host with a suitable redox potential, and the catalytic performance was evaluated (Fig. 1). We envisioned that the introduction of coordinated phosphorus atoms would help shift the redox potentials of the coordinated metal sites to more negative potentials, and these donor atoms could be engineered into this new complex to accelerate the photocatalytic hydrogen generation in combination with the selective hydrogenation of nitrobenzene to anilines. The experimental results indicated that the special redox-modulated environment of the host and the proximity effects of the host-guest interaction could promote the formation of the charge-transfer complex to decrease the overpotential and that the cofactor QHQ could accelerate the electron transfer outside the cavity to further improve the efficiency of selective nitroarene hydrogenation.

2. Results and discussion

Ligand H_4L^1 (5,5'-methylenebis(N^1, N^3 -bis(2-(diphenylphosphanyl)benzylidene)isophthalohydrazide)) was obtained by Schiff base reaction of 5,5'-methylenedi(isophthalohydrazide) with 2-(diphenylphosphanyl)benzaldehyde in an ethanol solution and characterized by elemental analysis and spectroscopic methods. The solution-phase stability of compound Co-L^1 and the host-guest behaviour of binding QHQ were characterized by electrospray ionization-mass spectrometry (ESI-MS). Three intense, sharp peaks at $m/z = 801.6560$, 974.3839 , and 1233.4789 (Fig. 2a) are assigned to $[\text{Co}_6(\text{L}^1)_3]^{6+}$, $[\text{Co}_6(\text{L}^1)_3\text{NO}_3^-]^{5+}$ and $[\text{Co}_6(\text{L}^1)_3\text{2NO}_3^-]^{4+}$, respectively, indicating the formation of the M_6L_3 species in solution. Co-L^1 was shielded by a total of forty-two benzene rings to form a spherical cavity, providing a hydrophilic environment for the encapsulation of the bio-inspired QHQ cofactor in the host. When five equiv. of QHQ was added into the acetonitrile solution of Co-L^1 , a new intense, sharp peak at $m/z = 1275.7515$ was observed, which could reasonably be attributed to a $[\text{Co}_6(\text{L}^1)_3(\text{QH}-2\text{H})\cdot\text{CH}_3\text{CN}\cdot 2\text{H}_2\text{O}]^{4+}$ species. A comparison of the experimentally obtained peak with that from the simulated natural isotopic abundances conforms to the formation of a 1:1 stoichiometric host-guest complex species $\text{Co-L}^1 \supset \text{QH}$ in solution (Fig. 2b).

The cyclic voltammogram of Co-L^1 suggested that the reduction processes of $\text{Co}^{\text{II}}/\text{Co}^{\text{I}}$ and $\text{Co}^{\text{III}}/\text{Co}^{\text{II}}$ occurred at approximately -1.41 and -0.69 V (vs. Ag/AgCl), respectively (Fig. 3a). Compared with the previously reported ONN chelators, the $\text{Co}^{\text{II}}/\text{Co}^{\text{I}}$ potential shifted 0.24 V towards more negative potential, which indicated that the compound Co-L^1 has higher reduction activity for hydrogen production [26]. This effect could be attributed to the introduction of “P” coordination sites in the Co-L^1 structure. The $\text{Co}^{\text{II}}/\text{Co}^{\text{I}}$ potential falls well within the potential range of proton reduction in aqueous media. After the addition of *p*-toluenesulfonic acid (0.8 mM) to the Co-L^1 solution, the voltammogram showed the appearance of a new peak at -1.57 V. Moreover, the intensity of the new wave increased with increasing concentrations of *p*-toluenesulfonic acid (Fig. 3a) [27]. The new wave was reasonably assigned to typical proton reduction, suggesting that Co-L^1 is capable of directly reducing protons in a catalytic reaction [28,29]. The appearance of these redox peaks proves that Co-L^1 can achieve proton reduction with high efficiency [30–32].

The Co-L^1 was firstly investigated as a catalyst for light-driven hydrogen production in a 20 mL flask. Under the optimized conditions,

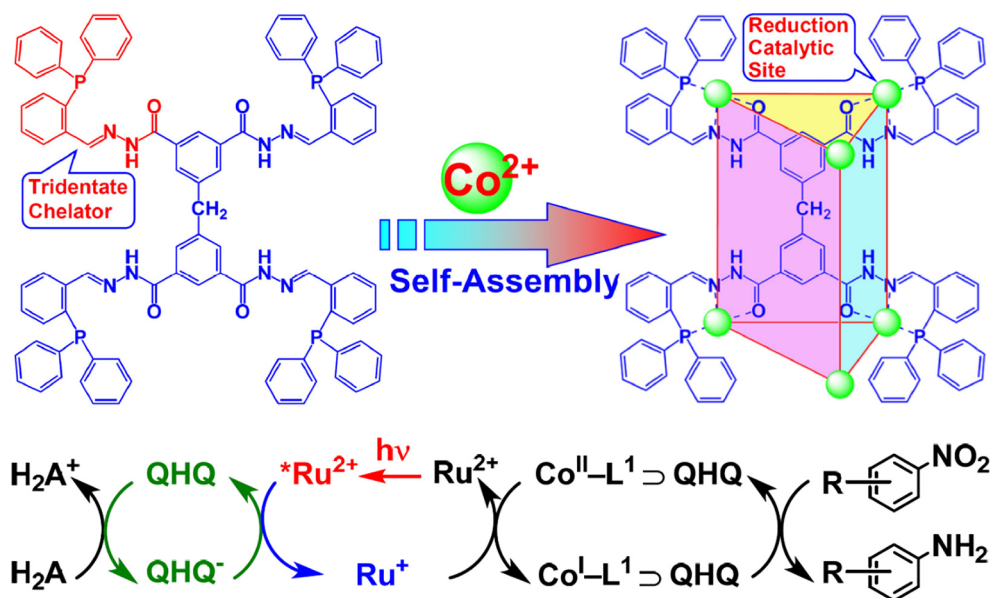


Fig. 1. Procedure for the synthesis of the metal-organic triangular prism and schematic representation of using a supramolecular system for the encapsulation of a quinoxaline cofactor within the cavity of the supramolecular triangular prism to combine light-driven proton reduction and selective hydrogenation of nitroarenes.

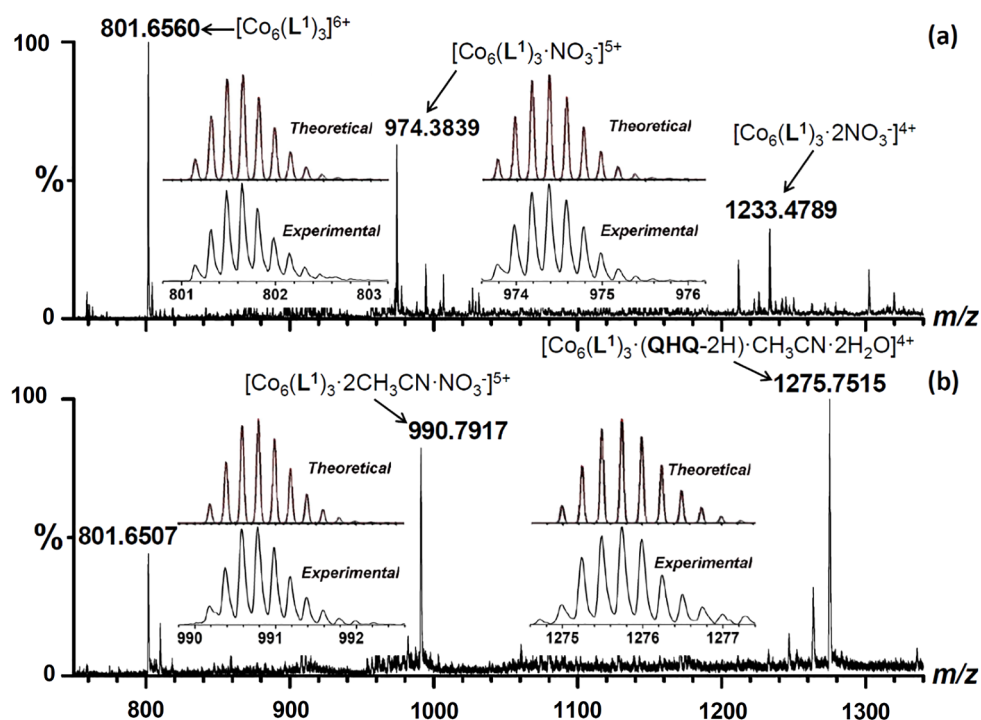


Fig. 2. ESI-MS spectra of (a) Co-L^1 and (b) Co-L^1 following the addition of 5 equiv. of QHQ in CH_3CN . The insets show the measured and simulated isotopic patterns at $m/z = 801.6560$, 974.3839 , 990.7917 and 1275.7515 .

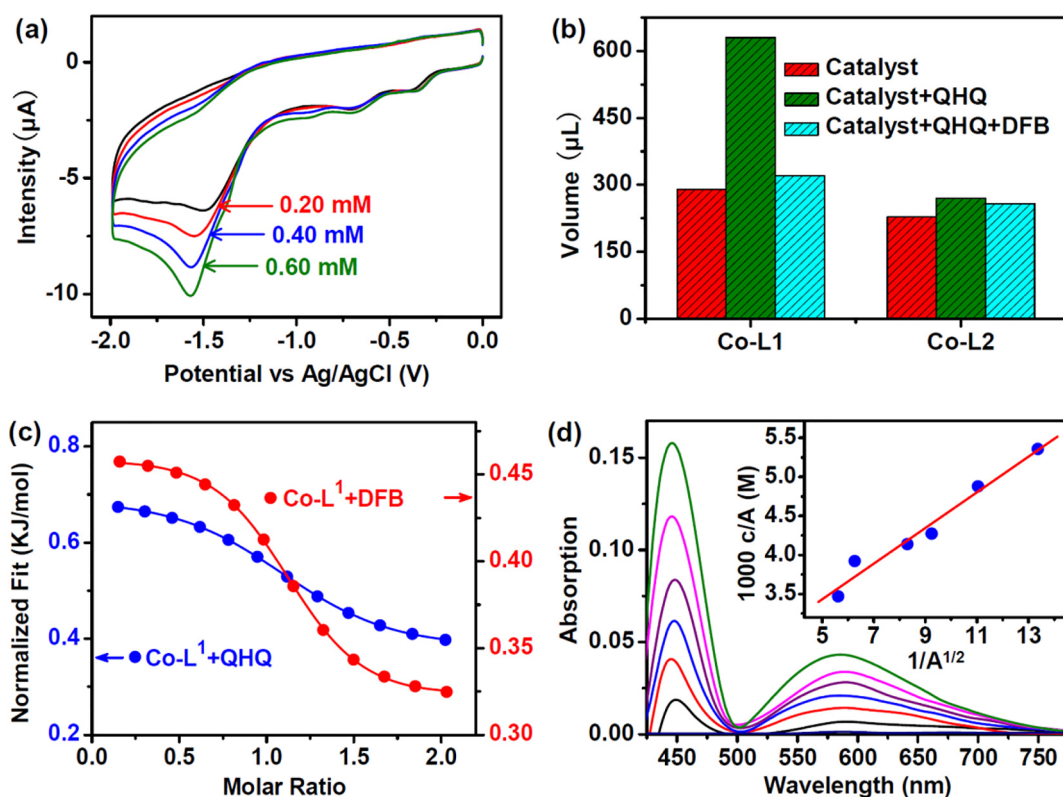


Fig. 3. (a) Cyclic voltammograms of Co-L^1 (0.1 mM) in CH_3CN containing 0.1 M TBAPF₆ (black line) and following the addition of *p*-toluenesulfonic acid. (b) Volume of hydrogen produced by the systems containing different catalysts (red bars, Co-L^1 : 2.5 μM , Co-L^2 : 15.0 μM), $\text{Ru}(\text{bpy})_3^{2+}$ (0.5 mM) and H_2A (0.1 M) in a $\text{CH}_3\text{CN}/\text{H}_2\text{O}$ solution (1:1, pH 4.75). The green and cyan bars show the hydrogen volumes generated by the systems containing QHQ (15 mM) and QHQ/DFB (15 mM/0.15 M), respectively. (c) ITC experiments on Co-L^1 upon the addition of QHQ or DFB showing the formation of host-guest complexes in CH_3CN . (d) UV-Vis absorption difference spectra of Co-L^1 (0.2 mM) in CH_3CN upon the addition of QHQ (0.3 mM). The insets show the linear plot of c/A against $1/A^{1/2}$ to estimate the association constant (K_a). (For interpretation of the references to colour in this figure legend, the reader is referred to the web version of this article.)

hydrogen was directly generated under continuous irradiation with a $\text{CH}_3\text{CN}/\text{H}_2\text{O}$ (1:1, v/v) solution containing $\text{Ru}(\text{bpy})_3^{2+}$ (0.5 mM), Co-L^1 (2.5 μM), and ascorbic acid (H_2A , 0.1 M) at a pH of 4.75 with light from a 500 W Xe lamp (Figs. S8–S10). The maximum volume of hydrogen produced reached 0.29 mL after 12 h (Fig. 3b) and was three times that of the previous similar system, except for the redox potential of the catalyst [25], indicating that the ONP chelators could regulate the potential of metal centres to facilitate proton reduction. Control experiments demonstrated that host Co-L^1 , photosensitizer $\text{Ru}(\text{bpy})_3^{2+}$ and electron donor H_2A are three indispensable elements for hydrogen generation. Of course, these proton reduction systems could not work well without light.

Under the optimized conditions, the addition of QHQ (15 mM) to the aforementioned reaction solution increased the hydrogen production to 0.62 mL (Fig. 3b) with an approximately 2200 of turnover number (TON), indicating that the formation of host-guest complex promotes occurrence of the hydrogen production (Fig. S11). Isothermal titration microcalorimetry (ITC) was used to ensure the quantitative accuracy of the relationship between the compound Co-L^1 and the cofactor QHQ as well as provide insight into the thermodynamics for host-guest complexation [33–35]. A typical titration curve is shown in Fig. 3c with the observed inclusion number 1 between Co-L^1 and QHQ. Curve fitting by the computer simulation using an “independent” model reveals an association constant of $2.92 \times 10^4 \text{ M}^{-1}$ with an activation enthalpy (ΔH) of $0.27 \text{ kJ}\cdot\text{mol}^{-1}$, activation entropy (ΔS) of $86.43 \text{ J}\cdot\text{mol}^{-1}$ and Gibbs free energy (ΔG) of $-25.50 \text{ kJ}\cdot\text{mol}^{-1}$ for $\text{Co-L}^1 \supset \text{QHQ}$ (Fig. S6). And the formation of host-guest charge-transfer complex was further demonstrated by UV/Vis differential absorption spectra, with a new absorption peak at 590 nm (Fig. 3d) [36]. The titration data result in the association constant of $3.20 \times 10^4 \text{ M}^{-1}$ for a 1:1 complex, which is in good consistent with the results in the ESI-MS and ITC spectra. Notably, Co-L^1 and QHQ have no absorption peak at this region, which suggests the formation of host-guest charge-transfer complexes. The results of the ESI-MS spectra, ITC, and UV/Vis spectra were mutually confirmed, indicating that a 1:1 mol ratio host-guest $\text{Co-L}^1 \supset \text{QHQ}$ cocrathration supramolecular system was formed stably in solution. Moreover, the addition of QHQ (0.2 mM) to a solution containing Co-L^1 (0.1 mM) resulted in a new irreversible peak at approximately -1.56 V (Fig. S13). This modified potential shifted 0.15 V towards more negative potential compared to the intrinsic potential (-1.41 V) of the compound Co-L^1 and may be attributable to the host-guest charge-transfer supramolecular system, which facilitates proton reduction more easily.

Under saturated reaction conditions, QHQ in high concentration ($K_{\text{ass}}[\text{QHQ}] > 100$) exhibited pseudo-zero-order kinetics of hydrogen production. The initial turnover frequency (TOF) of hydrogen production was no longer increased by further adding QHQ. When the concentration of QHQ was fixed at 15 mM, the TOF exhibited a linear relationship with the concentration of Co-L^1 in the range of 1.0 μM to 2.5 μM (Fig. 4a). However, the increase of multiples in TOF was more than that of the concentration of Co-L^1 . This result indicated that the TOF depends on the concentration of complex $\text{Co-L}^1 \supset \text{QHQ}$ and that excess QHQ could also accelerate the electron transfer to increase the TOF of hydrogen evolution outside the cavity. To further explore this type of system, the ligand HL^2 (N' -(2-(diphenylphosphanyl)benzylidene)benzohydrazide) was synthesized by benzhydrazide and 2-(diphenylphosphanyl)benzaldehyde and self-assembled with cobalt ions to generate a mononuclear cobalt complex Co-L^2 (Fig. S1). Then, control experiments of light-driven hydrogen generation were performed with Co-L^2 containing the same coordination configuration under the same conditions. The volumes of hydrogen generation were 0.23 and 0.27 mL for Co-L^2 instead of Co-L^1 in the absence and presence of the QHQ cofactor, respectively (Fig. 3b). An increase of 20% was observed, which was attributed to the ability of the QHQ cofactor to facilitate electron transfer in normal homogeneous systems. The superior hydrogen-evolving performance of the $\text{Co-L}^1/\text{QHQ}$ system over that of

the $\text{Co-L}^2/\text{QHQ}$ system is postulated to result from the well-defined host-guest interactions and the proximity effects created by the host architecture.

To further investigate the influence of the formation of host-guest charge-transfer complexes in the photocatalytic hydrogen evolution process, *p*-difluorobenzene (DFB), a redox-inactive species, was selected as an inhibitor for our enzymatic system. ITC curves of Co-L^1 after adding DFB revealed the formation of a host-guest system with an association constant of 3.93×10^4 (Figs. 3c and S7). The higher binding constant than that of the $\text{Co-L}^1/\text{QHQ}$ system indicates that DFB could replace QHQ and be encapsulated in the pocket of the capsule. As expected, hydrogen production sustained only an increase of 10% in the presence of QHQ (15 mM) and DFB (0.15 M) (Fig. 4b). However, when DFB was added to the $\text{Co-L}^2/\text{QHQ}$ reaction system, there was no significant influence on hydrogen production (Fig. 3b). The continual catalysis of similar molecules is unique to enzyme systems, and the results indicated that the catalytic effect of the system is inhibited due to the presence of host-guest complexes.

The introduction of the ONP chelators endows these metal-organic supramolecular systems with an appropriate redox potential to allow photocatalytic reduction of protons to form active H-atoms that can selectively reduce reaction intermediates or substrates [37,38]. In a typical model reaction, *p*-nitroacetophenone with bifunctional groups was used as the substrate for the selective reduction of the nitro group. The addition of 40 mM *p*-nitroacetophenone to a solution containing Co-L^1 (2.5 μM), H_2A (0.1 M), and $\text{Ru}(\text{bpy})_3^{2+}$ (0.5 mM) resulted in a 33% yield, and the selectivity of the product *p*-aminoacetophenone reached 99%. Under the same conditions, with the addition of QHQ (15 mM) to the aforementioned reaction solution, a yield of 48% with a turnover number (TON) of 7700 per mole of catalyst was obtained, and the TOF was as high as 650 per mole of catalyst per hour. After 12 h of irradiation, only a trace amount of *p*-nitrophenylmethanol was detected, and the hydrogen evolution was stopped, which suggested that this supramolecular system was highly efficient and stable. Interestingly, when the concentration of Co-L^1 was fixed at 2.5 μM , the TOF of the photocatalytic reduction of *p*-nitroacetophenone increased with increasing QHQ concentration, and the TON reached a maximum of 11,600 at 30 mM. However, the TOF as high as 970 per mole of catalyst per hour remained unchanged when the QHQ concentration continued to increase (50 mM) (Fig. 4c). We speculated that a high concentration of substrate could inhibit the formation of the $\text{Co-L}^1 \supset \text{QHQ}$ host-guest complexes to influence the reaction efficiency (Fig. S5).

To demonstrate the general applicability of our catalyst system, various nitroarenes were tested (Table 1). The results showed that the carbonyl group cannot be reduced due to the insufficient reduction potential of both the photosensitizer and the host-guest complex. The selectivity of all corresponding amino products reached 99% with high TON values. For a time-course experiment, an excess of *p*-nitroacetophenone (0.1 M) was added, and H_2A was added into the reaction system halfway through the experiment to ensure that the H_2A concentration remained at 0.1 M. After 60 h, the TON value reached 18,000. Most importantly, when QHQ (30 mM) was added to the system, the TON value reached 36,000 through 6 superimposed experiments (Fig. 4d).

3. Conclusions

In summary, a new strategy for the construction of a host-guest charge-transfer system was further developed to accelerate photocatalytic hydrogen generation and the selective hydrogenation of nitroarenes. The approach included the self-assembly of the well-designed redox-active metal-organic prism host, which has a suitable pocket size and a special redox-modulated environment to encapsulate the QHQ cofactor, benefitting the formation of a charge-transfer complex. The enhanced electron transfer efficiency due to the proximity effects of the host-guest systems, the well-localized redox events and the electron

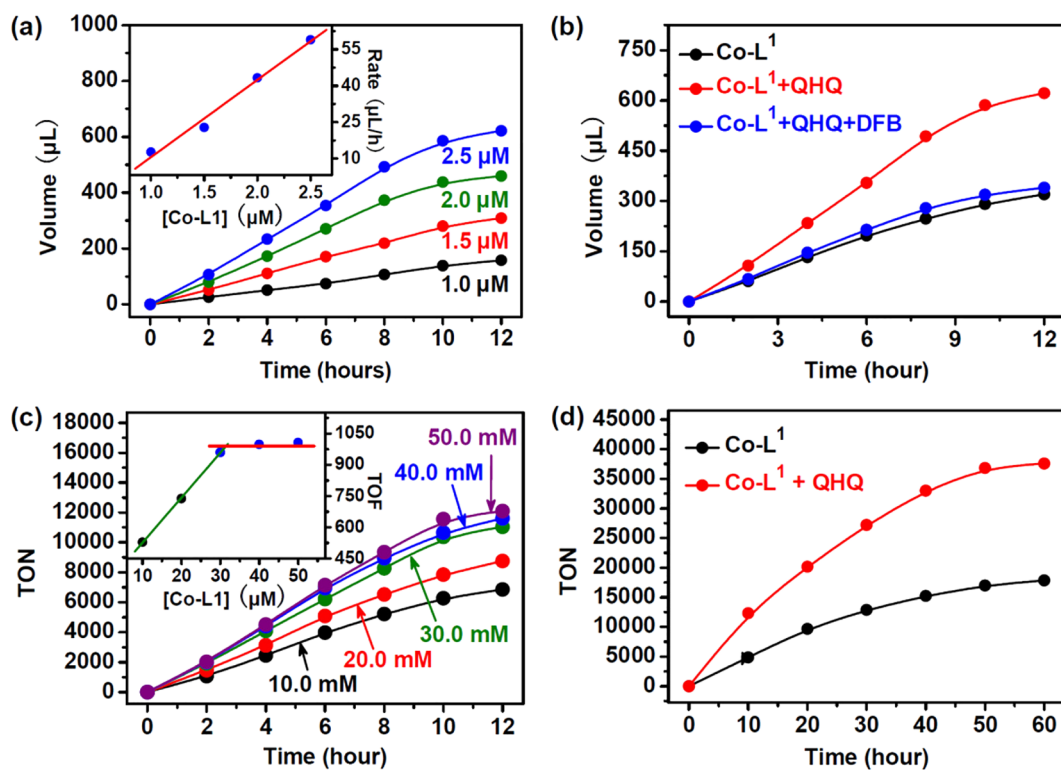
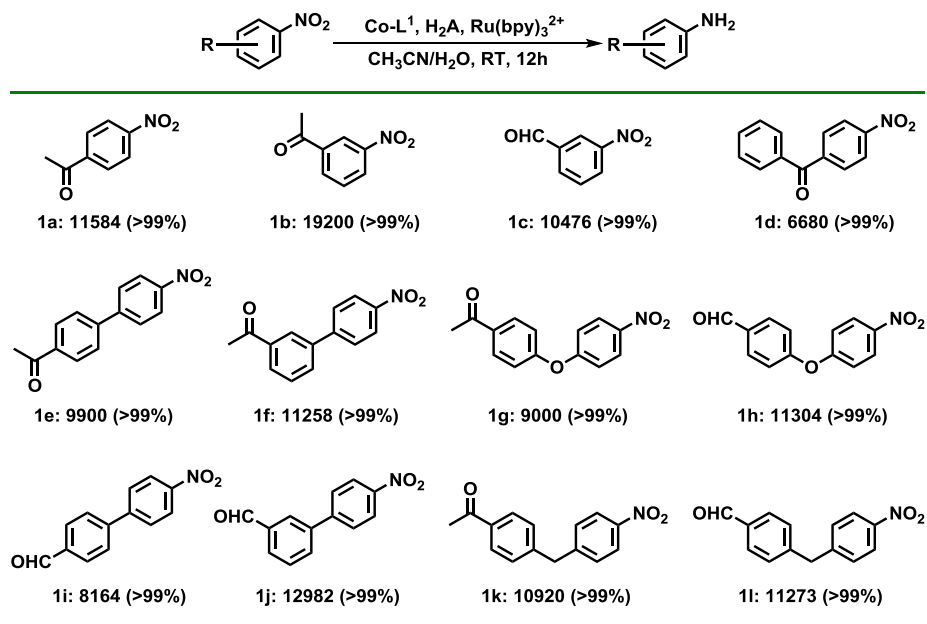


Fig. 4. (a) Light-driven hydrogen evolution of systems containing QHQ (15 mM), Ru(bpy)₃²⁺ (0.5 mM), H₂A (0.10 M) in a CH₃CN/H₂O solution (1:1, pH = 4.75) with different concentrations of Co-L¹. The insets show the linear plot of the hydrogen production rate against the concentration of Co-L¹. (b) Light-driven hydrogen evolution of the system containing Ru(bpy)₃²⁺ (0.5 mM), H₂A (0.1 M), and Co-L¹ (2.5 μM) in CH₃CN/H₂O (1:1, pH 4.75, black line) and following the addition of 15 mM QHQ (red line) or both 15 mM QHQ and 0.15 M DFB (blue line). (c) Light-driven selective nitro reduction of the system containing *p*-nitroacetophenone (40 mM), Ru(bpy)₃²⁺ (0.5 mM), H₂A (0.1 M), Co-L¹ (2.5 μM) in CH₃CN/H₂O (1:1, pH = 4.75) with different concentrations of QHQ. The insets show the linear plot of TOF against the concentration of Co-L¹. (d) Light-driven selective nitro reduction of the system containing *p*-nitroacetophenone (0.1 M), Ru(bpy)₃²⁺ (0.5 mM), H₂A (0.1 M), and Co-L¹ (2.5 μM) in CH₃CN/H₂O (1:1, pH = 4.75, black line) and following the addition of 30 mM QHQ (red line). (For interpretation of the references to colour in this figure legend, the reader is referred to the web version of this article.)

Table 1

The selective reduction of nitroarenes^a.



^aReaction conditions: Substrate (40 mM), Co-L¹ (2.5 μM), Ru(bpy)₃²⁺ (0.5 mM), H₂A (0.1 M), and QHQ (30 mM) in CH₃CN/H₂O (1:1, pH = 4.75), 12 hours. The TON was determined by GC-MS analysis of the crude products.

transfer effect of QHQ outside the metal-organic prism cavity allow the tandem reductions to proceed to efficiently reduce the nitro group using active H-sources from photo-activated water. The excellent activity and improved stability suggest that the novel approach for the construction of supramolecular systems as efficient homogeneous catalysts is promising and could be extended to other hydrogenation transformations using light as a clean energy source.

4. Experimental

4.1. Materials and methods

All the chemicals and solvents were of reagent grade quality obtained from commercial sources and used without further purification. The elemental analyses of C, H and N were performed on a Vario EL III elemental analyzer. ^1H NMR spectra were collected on a Bruker 400 M spectrometer. ESI mass spectra were obtained from an HPLC-Q-T of mass spectrometer using acetonitrile as the mobile phase. UV-vis spectra were collected on an HP 8453 spectrometer. The fluorescence emission spectra were collected on an Edinburgh FS920. Isothermal Titration Calorimetry (ITC) were performed on a Nano ITC (TA Instruments Inc. -Waters LLC). The solution of $\text{Ru}(\text{bpy})_3(\text{PF}_6)_2$ was prepared in CH_3CN .

Electrochemical measurements were performed with a ZAHNER ZENNIUM electrochemical workstation with a conventional three-electrode system with a custom-designed Ag/AgCl electrode as a reference electrode, a platinum silk with 0.5 mm diameter as a counter electrode, and glassy carbon electrode as a working electrode. Cyclic voltammograms with the solution concentrations were 0.10 mM for the cobalt-based compounds and 0.10 M (*n*-Bu₄N)PF₆ for the supporting electrolyte. Electrodes were polished on a MD-Nap polishing pad. Additions of *p*-toluene sulfonic acid were made by syringe using a 0.10 M solution in CH_3CN . The measurements were performed at room temperature after the system had been degassed with argon.

4.2. General procedure for hydrogen production

In a typical experiment, photoinduced hydrogen evolution was made in a 20 mL flask. Varying amounts of the catalyst, $\text{Ru}(\text{bpy})_3^{2+}$ and ascorbic acid in 1:1 $\text{CH}_3\text{CN}/\text{H}_2\text{O}$ were added to obtain a total volume of 5.0 mL. The flask was sealed with a septum, degassed by bubbling argon for 15 min under atmospheric pressure at room temperature. The pH of this solution was adjusted to a specific pH by adding H_2SO_4 or NaOH and measured with a pH meter. After that, the samples were irradiated by a 500 W Xenon Lamp, the reaction temperature was 298 K by using a water filter to absorb heat. The generated photoproduct of H_2 was characterized using a GC 7890 T gas chromatograph equipped with a 5 Å molecular sieve column (0.6 m × 3 mm) and a thermal conductivity detector; argon was used as the carrier gas. The amount of hydrogen generated was determined by the external standard method. Hydrogen in the resulting solution was not measured and the slight effect of the hydrogen gas generated on the pressure of the flask was neglected for calculation of the volume of hydrogen gas [39].

4.3. General procedure for selective hydrogenation of nitroarenes to anilines

In a typical experiment, selective hydrogenation of nitroarenes to anilines was made in a 20 mL flask. Varying amounts of the *p*-nitroacetophenone, the catalyst, $\text{Ru}(\text{bpy})_3^{2+}$ and ascorbic acid in 1:1 $\text{CH}_3\text{CN}/\text{H}_2\text{O}$ were added to obtain a total volume of 5.0 mL. The flask was sealed with a septum, degassed by bubbling argon for 15 min under atmospheric pressure at room temperature. The pH of this solution was adjusted to a specific pH by adding H_2SO_4 or NaOH and measured with a pH meter. After that, the samples were irradiated by a 500 W Xenon Lamp, the reaction temperature was 298 K by using a water filter to absorb heat. The generated photoproduct of selective hydrogenation of

nitroarenes evolution was characterized by GC-MS analysis.

5. Preparation and characterizations

5.1. Synthesis of H_4L^1

A 250 mL round-bottomed flask equipped with magnetic stir bar and reflux condenser was charged with 5,5'-methylene-diisophthalohydrazide (2.00 g, 5.00 mmol) [40], 2-(Diphenylphosphino)benzaldehyde (6.39 g, 22.00 mmol) and 150 mL ethanol. The mixture was heated at boiling temperature under magnetic stirring for 12 h. A white precipitate was formed, which was collected by filtration and dried in vacuum. Yield: 6.50 g, 87.3%. ^1H NMR (400 MHz, DMSO-*d*₆, ppm) δ 12.11 (s, 4H_{NH}), 8.24 (s, 2H_{benzene}), 8.07 (d, *J* = 4.8 Hz, 4H_{benzene}), 7.98 (s, 4H_{benzene}), 7.83 (s, 4H_{CH}), 7.55 (t, *J* = 4.8 Hz, 4H_{benzene}), 7.51 (t, *J* = 6.0 Hz, 8H_{benzene}), 7.34–7.41 (m, 24H_{benzene}), 7.19 (d, *J* = 1.6 Hz, 16H_{benzene}), 4.08 (s, 2H_{CH2}). Elemental analysis calcd for C₉₃H₇₂N₈O₄P₄: H 4.87, C 74.99, N 7.52%. Found: H 4.90, C 74.41, N 7.47%. ESI-MS calcd for C₉₃H₇₂N₈O₄P₄ 1489.4659, found 1512.5895 [M + Na]⁺, 1528.5942 [M + K]⁺.

5.2. Preparation of Co-L¹

A solution of Co(NO₃)₂·6H₂O (58.21 mg, 0.20 mmol) and H₄L¹ (74.48 mg, 0.05 mmol) in CH₃OH/CH₃CN/C₂H₅OH (1:1:1, 30 mL) was stirred for 2 h at room temperature. Then the solution was left for several weeks at room temperature to give red solid. Yield: 49.61 mg, 53.4%. Elemental analysis calcd for Co₆C₂₇₉H₂₀₆N₂₄O₁₂P₁₂8NO₃·5C₂H₅OH·H₂O: H 4.32, C 62.47, N 8.07%. Found: H 4.52, C 62.78, N 7.80%. ESI-MS: *m/z*: 801.6560 [Co₆(L¹)₃]⁶⁺, 974.3839 [Co₆(L¹)₃NO₃]⁵⁺ and 1233.4789 [Co₆(L¹)₃2NO₃]⁴⁺.

5.3. Synthesis of benzhydrazide

A 250 mL round-bottomed flask equipped with magnetic stir bar and reflux condenser was charged with 80% hydrazine hydrate (16 mL), ethyl benzoate (1.50 g, 10.00 mmol) and 100 mL ethanol. The mixture was heated at boiling temperature under magnetic stirring for 24 h. A white precipitate was formed, which was collected by filtration and dried in vacuum. Yield: 1.24 g, 91.1%. ^1H NMR (400 MHz, DMSO-*d*₆, ppm) δ 9.75 (s, 1H_{NH}), 7.82 (d, *J* = 6.4 Hz, 2H_{benzene}), 7.51 (t, *J* = 5.6 Hz, 1H_{benzene}), 7.44 (t, *J* = 6.0 Hz, 2H_{benzene}), 4.48 (s, 2H_{NH2}). Elemental analysis calcd for C₇H₈N₂O: H 5.92, C 61.75, N 20.58%. Found: H 6.17, C 59.83, N 19.67%. ESI-MS calcd for C₇H₈N₂O: 136.0637, found 137.0721 [M + H]⁺, 159.0514 [M + Na]⁺.

5.4. Synthesis of HL²

A 250 mL round-bottomed flask equipped with magnetic stir bar and reflux condenser was charged with benzhydrazide (0.68 g, 5.00 mmol), 2-(diphenylphosphino)benzaldehyde (1.60 g, 5.50 mmol) and 150 mL ethanol. The mixture was heated at boiling temperature under magnetic stirring for 12 h. A white precipitate was formed, which was collected by filtration and dried in vacuum. Yield: 1.83 g, 89.6%. ^1H NMR (400 MHz, DMSO-*d*₆, ppm) δ 12.01 (s, 1H_{NH}), 9.19 (d, *J* = 3.6 Hz, 1H_{benzene}), 8.09 (s, 1H_{CH}), 7.89 (d, *J* = 5.6 Hz, 2H_{benzene}), 7.58 (d, *J* = 4.8 Hz, 1H_{benzene}), 7.46–7.54 (m, 3H_{benzene}), 7.38–7.44 (m, 7H_{benzene}), 7.22 (d, *J* = 3.2 Hz, 4H_{benzene}), 6.85 (t, *J* = 4.8 Hz, 1H_{benzene}). Elemental analysis calcd for C₂₆H₂₁N₂O: H 5.18, C 76.46, N 6.86%. Found: H 5.29, C 75.39, N 6.75%. ESI-MS calcd for C₂₆H₂₁N₂O: 408.1391, found 409.1485 [M + H]⁺, 431.1318 [M + Na]⁺.

5.5. Preparation of Co-L²

A solution of Co(NO₃)₂·6H₂O (29.10 mg, 0.10 mmol) and HL²

(40.84 mg, 0.10 mmol) in CH₃OH/CHCl₃ (1:1, 10 mL) was stirred for 2 h at room temperature. Then the solution was left for several days at room temperature to give orange solid. The solid were dried in vacuum. Yield: 28.14 mg, 56.1%. Elemental analysis calcd for Co (C₂₆H₂₀N₂OP)₂NO₃·CH₃OH·2H₂O: H 4.82, C 63.41, N 6.98%. Found: H 4.87, C 63.13, N 6.91%. ESI-MS: *m/z*: 873.2084 [Co(L²)₂]⁺.

Acknowledgements

This work was supported by the National Natural Science Foundation of China (No. 21531001 and 21820102001) and the Fundamental Research Funds for the Central Universities (DUT18LK53 and DUT19ZD102).

Appendix A. Supplementary data

Supplementary data to this article can be found online at <https://doi.org/10.1016/j.inoche.2019.107558>.

References

- H.U. Blaser, H. Steiner, M. Studer, Selective catalytic hydrogenation of functionalized nitroarenes: an update, *Chem. Cat. Chem.* 1 (2009) 210–221.
- X.J. Yang, B. Chen, L.Q. Zheng, L.Z. Wu, C.H. Tung, Highly efficient and selective photocatalytic hydrogenation of functionalized nitrobenzenes, *Green Chem.* 16 (2014) 1082–1086.
- G. Liang, A. Wang, L. Li, G. Xu, N. Yan, T. Zhang, Production of primary amines by reductive amination of biomass-derived aldehydes/ketones, *Angew. Chem. Int. Ed.* 56 (2017) 3050–3054.
- A. Mukherjee, D. Srimani, S. Chakraborty, Y. Ben-David, D. Milstein, Selective hydrogenation of nitriles to primary amines catalyzed by a cobalt pincer complex, *J. Am. Chem. Soc.* 137 (2015) 8888–8891.
- S. Elangovan, C. Topf, S. Fischer, H. Jiao, A. Spangenberg, W. Baumann, R. Ludwig, K. Junge, M. Beller, Selective catalytic hydrogenations of nitriles, ketones, and aldehydes by well-defined manganese pincer complexes, *J. Am. Chem. Soc.* 138 (2016) 8809–8814.
- E.J. Derrah, M. Hanauer, P.N. Plessow, M. Schelwies, M.K. da Silva, T. Schaub, Ru (II)-triphos catalyzed amination of alcohols with ammonia via ionic species, *Organometallics* 34 (2015) 1872–1881.
- M. Ousmane, G. Perrussel, Z. Yan, J.M. Clacens, F. De Campo, M. Pera-Titus, Highly selective direct amination of primary alcohols over a Pd/K-OMS-2 catalyst, *J. Catal.* 309 (2014) 439–452.
- J. Mao, W. Chen, W. Sun, Z. Chen, J. Pei, D. He, C. Lv, D. Wang, Y. Li, Rational control of the selectivity of a ruthenium catalyst for hydrogenation of 4-nitrostyrene by strain regulation, *Angew. Chem. Int. Ed.* 56 (2017) 11971–11975.
- J. Zhang, L. Wang, Y. Shao, Y. Wang, B.C. Gates, F.-S. Xiao, A Pd@zeolite catalyst for nitroarene hydrogenation with high product selectivity by sterically controlled adsorption in the zeolite micropores, *Angew. Chem. Int. Ed.* 56 (2017) 9747–9751.
- C.J. Brown, F.D. Toste, R.G. Bergman, K.N. Raymond, Supramolecular catalysis in metal–ligand cluster hosts, *Chem. Rev.* 115 (2015) 3012–3035.
- K. Yan, M. Fujita, A speedy marriage in supramolecular catalysis, *Science* 350 (2015) 1165–1166.
- R.J. Hooley, Taking on the turnover challenge, *Nat. Chem.* 8 (2016) 202–204.
- D. Zhang, A. Martinez, J.P. Dutasta, Emergence of hemicryptophanes: from synthesis to applications for recognition, molecular machines, and supramolecular catalysis, *Chem. Rev.* 117 (2017) 4900–4942.
- M. Pan, K. Wu, J.H. Zhang, C.Y. Su, Chiral metal–organic cages/containers (MOCs): from structural and stereochemical design to applications, *Coord. Chem. Rev.* 378 (2019) 333–349.
- L. Zhao, X. Jing, X. Li, X. Guo, L. Zeng, C. He, C. Duan, Catalytic properties of chemical transformation within the confined pockets of Werner-type capsules, *Coord. Chem. Rev.* 378 (2019) 151–187.
- D.M. Kaplan, M.D. Levin, R.G. Bergman, K.N. Raymond, F.D. Toste, A supramolecular microenvironment strategy for transition metal catalysis, *Science* 350 (2015) 1235–1238.
- Q.Q. Wang, S. Gonell, S.H.A.M. Leenders, M. Dürr, I. Ivanović-Burmazović, J.N.H. Reek, Self-assembled nanospheres with multiple endohedral binding sites pre-organize catalysts and substrates for highly efficient reactions, *Nat. Chem.* 8 (2016) 225–230.
- H. Takezawa, T. Kanda, H. Nanjo, M. Fujita, Site-selective functionalization of linear diterpenoids through U-shaped folding in a confined artificial cavity, *J. Am. Chem. Soc.* 141 (2019) 5112–5115.
- T.R. Cook, P.J. Stang, Recent developments in the preparation and chemistry of metallocycles and metallacages via coordination, *Chem. Rev.* 115 (2015) 7001–7045.
- P.A. Frey, Coenzymes and radicals, *Science* 294 (2001) 2489–2490.
- M.D. White, K.A.P. Payne, K. Fisher, S.A. Marshall, D. Parker, N.J.W. Rattray, D.K. Trivedi, R. Goodacre, S.E.J. Rigby, N.S. Scrutton, S. Hay, D. Leys, UbiX is a flavin prenyltransferase required for bacterial ubiquinone biosynthesis, *Nature* 522 (2015) 502–506.
- A. Bhagi-Damodaran, M.A. Michael, Q. Zhu, J. Reed, B.A. Sandoval, E.N. Mirts, S. Chakraborty, P. Moënn-Loccoz, Y. Zhang, Y. Lu, Why copper is preferred over iron for oxygen activation and reduction in haem-copper oxidases, *Nat. Chem.* 9 (2016) 257–263.
- H.M. Peng, R.J. Auchus, Molecular recognition in mitochondrial cytochromes P450 that catalyze the terminal steps of corticosteroid biosynthesis, *Biochemistry* 56 (2017) 2282–2293.
- J. Regeimbal, S. Gleiter, B.L. Trumppower, C.A. Yu, M. Diwakar, D.P. Ballou, J.C.A. Bardwell, Disulfide bond formation involves a quinhydrone-type charge-transfer complex, *Proc. Natl. Acad. Sci. U. S. A.* 100 (2003) 13779–13784.
- L. Zhao, J. Wei, J. Zhang, C. He, C. Duan, Encapsulation of a quinhydrone cofactor in the inner pocket of cobalt triangular prisms: combined light-driven reduction of protons and hydrogenation of nitrobenzene, *Angew. Chem. Int. Ed.* 56 (2017) 15284–15288.
- C. Baffert, V. Artero, M. Fontecave, Cobaloximes as functional models for hydrogenases. 2. Proton electroreduction catalyzed by difluoroborylbis(dimethylglyoximate)cobalt(II) complexes in organic media, *Inorg. Chem.* 46 (2007) 1817–1824.
- V. Artero, M. Chavarot-Kerlidou, M. Fontecave, Splitting water with cobalt, *Angew. Chem. Int. Ed.* 50 (2011) 7238–7266.
- X.Y. Dong, M. Zhang, R.B. Pei, Q. Wang, D.H. Wei, S.Q. Zang, Y.T. Fan, T.C.W. Mak, A crystalline copper(II) coordination polymer for the efficient visible-light-driven generation of hydrogen, *Angew. Chem. Int. Ed.* 55 (2016) 2073–2077.
- H.I. Karunadasa, C.J. Chang, J.R. Long, A molecular molybdenum-oxo catalyst for generating hydrogen from water, *Nature* 464 (2010) 1329–1333.
- J. Song, Z.F. Huang, L. Pan, K. Li, X. Zhang, L. Wang, J.J. Zou, Review on selective hydrogenation of nitroarene by catalytic, photocatalytic and electrocatalytic reactions, *Appl. Catal., B* 227 (2018) 386–408.
- P.H. Given, M.E. Peover, J. Schoen, 547. Polarography of some aromatic carbonyl compounds in dimethylformamide, *J. Chem. Soc.* (1958) 2674–2679.
- Y. Zhu, J. Zhang, Z. Chen, A. Zhang, C. Ma, Synthesis of nitrocarbazole compounds and their electrocatalytic oxidation of alcohol, *Chin. J. Catal.* 37 (2016) 533–538.
- S.F.M. van Dongen, S. Cantekin, J.A.A.W. Elemans, A.E. Rowan, R.J.M. Nolte, Functional interlocked systems, *Chem. Soc. Rev.* 43 (2014) 99–122.
- X. Ma, H. Tian, Bright functional rotaxanes, *Chem. Soc. Rev.* 39 (2010) 70–80.
- S. Kaabel, J. Adamson, F. Topić, A. Kiesilä, E. Kalenius, M. Öeren, M. Reimund, E. Prigorchenko, A. Löökene, H.J. Reich, K. Rissanen, R. Aav, Chiral hemicucurbit [8]uril as an anion receptor: selectivity to size, shape and charge distribution, *Chem. Sci.* 8 (2017) 2184–2190.
- A. Das, S. Ghosh, Supramolecular assemblies by charge-transfer interactions between donor and acceptor chromophores, *Angew. Chem. Int. Ed.* 53 (2014) 2038–2054.
- Z. Han, R. Eisenberg, Fuel from water: the photochemical generation of hydrogen from water, *Acc. Chem. Res.* 47 (2014) 2537–2544.
- L. Zhao, J. Wei, J. Lu, C. He, C. Duan, Renewable molecular flasks with NADH models: combination of light-driven proton reduction and biomimetic hydrogenation of benzoxazinones, *Angew. Chem. Int. Ed.* 56 (2017) 8692–8696.
- J. Dong, M. Wang, P. Zhang, S. Yang, J. Liu, X. Li, L. Sun, Promoting effect of electrostatic interaction between a cobalt catalyst and a xanthene dye on visible-light-driven electron transfer and hydrogen production, *J. Phys. Chem. C* 115 (2011) 15089–15096.
- M. Mazik, A. König, Mimicking the binding motifs found in the crystal structures of protein–carbohydrate complexes: an aromatic analogue of serine or threonine side chain hydroxyl/main chain amide, *Eur. J. Org. Chem.* 2007 (2007) 3271–3276.